



The development of the bending test machine prototype for wood and bamboo structures

Jonathan Bryan^a, Raditya Edra Raja Handika^a, Jarvis Eros Lananggalih^a, Michael Harlen^a, Sean Nabill Van Der Heijden^a, Farid Triawan^a, Kushendarsyah Saptaji^a, Ignatius Budi Sutanto Hadisujoto^a

^aSampoerna University Jakarta, Indonesia

Email of the corresponding author: jonathan.bryan@my.sampoernauniversity.ac.id

Abstract

This study presents the development of a low-cost, portable bending test machine specifically designed to evaluate the mechanical properties of wood and bamboo, with a focus on providing an accessible solution for small-scale users and researchers. The machine employs a standard three-point bending configuration, equipped with digital sensors to capture accurate load and deflection data. Meanwhile, an automated grading algorithm facilitates objective assessment. The prototype was modelled in SOLIDWORKS for precision in design and subsequently fabricated using a combination of wood and 3D-printed Polylactic acid (PLA) components to ensure affordability and portability. A Raspberry Pi microcontroller was integrated to enable real-time data acquisition and processing, enhancing usability in both laboratory and field settings. Through optimized linear regression supported by Singular Value Decomposition (SVD), the system calculates effective critical mechanical properties such as Young's modulus with a high degree of accuracy. This innovation provides a practical, efficient, and user-friendly alternative to conventional testing equipment, offering significant potential for material classification, quality control, and advancing sustainable construction practices by promoting the use of renewable resources like wood and bamboo.

Keywords: bending test, machine manufacture, stress analysis, structural test, wood and bamboo

1. Introduction

The bending test functions as an essential technique to assess material mechanical properties when subjected to flexural stresses. This testing method provides vital information about material strength and is commonly used to evaluate biological structures, such as bones, and engineering elements, like beams. The bending test typically exists in two fundamental setups: the three-point and four-point configurations. While both share similar mechanisms, they differ in the distribution of applied forces. The three-point bending test, in particular, is favoured for its simplicity and affordability, making it highly suitable for educational laboratories and low-budget facilities [1], [2]. Building upon its practicality, the three-point bending test is widely recognized for its effectiveness in measuring Young's modulus with notable accuracy, as well as its ease in specimen preparation and equipment setup. These features make it an efficient method for a quick analysis of mechanical properties across various engineering contexts, as supported by Martin-Nelson et al. Although the stress distribution in this method is less uniform compared to the four-point test, the three-point bending test remains a practical evaluation tool due to its balance of precision, simplicity, and cost-effectiveness [3], [4], [5].

Given this utility, bamboo, as a sustainable material known for its structural applications, is frequently tested using bending methods to determine its flexural strength and optimize its implementation in construction. Studies suggest that bamboo particleboard can outperform eucalyptus-based alternatives in bending strength,

reinforcing bamboo's position as a viable green building material [6], [7]. However, like many natural materials, the mechanical properties of bamboo are influenced by sample dimensions. Larger specimens often exhibit reduced strength due to inherent imperfections, such as knots and cavities. Consequently, size effect laws such as the Size Effect Law (SEL) and the Bažant Energetic Method (BEM) are employed to understand how tensile strength and fracture toughness vary with size [8]. One notable species, Moso bamboo, is prized for its high strength-to-weight ratio, positioning it as a potential lightweight alternative to steel. Despite having lower absolute bending strength, its renewable nature and reduced weight make it attractive for sustainable engineering solutions [9]. The bending behaviour of bamboo beams is further shaped by factors such as interfacial slippage, which can be improved with reinforcements like steel bands or composite layering. Bamboo's anisotropic properties—where strength varies depending on the direction of applied stress—further emphasize the need for targeted structural design, allowing engineers to harness its potential more effectively in load-bearing applications [10], [11].

Research by David Trujillo and colleagues has shown that combining bamboo with concrete enhances its mechanical performance. Their four-point bending tests on Guadua angustifolia Kunth demonstrated improved flexural strength and elasticity, showcasing the promise of bamboo-composite configurations in structural applications [3], [11]. Furthermore, bamboo's bending strength varies along its height due to changes in fibre density and distribution. Higher fibre volumes near the top sections of culms correlate with increased modulus of rupture (MOR) and modulus of elasticity (MOE), underscoring the importance of understanding bamboo's internal variability when evaluating its structural performance [12], [13]. Due to bamboo's hollow structure, it is also more prone to shear failure at support points, reinforcing the importance of reliable bending tests for structural assessment [14], [15]. To address variability and ensure consistent application, bamboo grading through standardized bending tests is crucial. ISO 19624:2018 provides formal procedures to assess bamboo's mechanical properties. For example, studies of Italian bamboo species used four-point bending tests and ANOVA analysis to statistically group specimens based on mechanical strength rather than taxonomy, allowing more practical material selection for construction [16], [17]. Similarly, grading of Phyllostachys edulis into strength classes based on MOE and bending strength further validates the reliability of these testing methods in distinguishing material quality [16].

With the increasing demand for accessible testing, developing an automated bending test machine becomes a practical solution. The Raspberry Pi 4 stands out as a suitable controller for such systems, offering robust computational performance, efficient multitasking capabilities, and real-time data visualization. Compared to platforms like Arduino Uno or ESP32, it enables easier integration with cloud-based monitoring systems, making it ideal for low-cost automated setups [18]. The choice of actuator also plays a critical role in the bending test of the machine's function. Hydraulic actuators, though powerful, require intensive maintenance and carry environmental risks due to potential fluid leakage. Pneumatic options offer cleanliness and simplicity but lack precise force control. In contrast, electric actuators strike a balance by providing accurate force application and energy efficiency, making them ideal for automated bending systems, especially in resource-constrained settings [19].

To further enhance system capabilities, integrating acoustic emission (AE) sensors allows for real-time structural health monitoring by detecting micro-crack formation and fibre fracture events. These non-destructive sensors simplify instrumentation while

significantly improving damage detection. Alternative sensing technologies, such as laser displacement and ultrasonic sensors, also contribute value, with laser systems providing high-precision deformation tracking and ultrasonic sensors offering affordable, general-purpose measurement solutions [20], [21], [22], [23], [24]. Given the limitations of conventional testing equipment, a cost-effective bending test machine priced below 10 million rupiah could be transformative for small-scale users, particularly bamboo farmers and rural industries. Current market machines, ranging from US \$10,000 to \$1,000,000, remain financially inaccessible to many. An affordable, reliable alternative would democratize material testing, enhance the credibility and value of bamboo products, and support broader adoption of sustainable materials in construction and manufacturing [25], [26].

The mechanical properties of bamboo and wood vary significantly depending on species, growth conditions, and processing methods, making material selection for agricultural applications a challenge, especially due to the lack of standardized and accessible testing methods. Existing bending test machines are often costly, complex, or suited for industrial-scale use, which limits their practicality for small-scale users such as farmers, craftsmen, and researchers. To address this gap, the objective is to design and develop a cost-effective, user-friendly bending test machine specifically tailored for bamboo used in agricultural settings. In addition to generating reliable material strength data, the machine will support efficient material grading. It is an essential process for optimizing resource use, improving structural performance, and ensuring trade consistency. By simplifying test procedures and data interpretation, the machine aims to enhance the accuracy and accessibility of bamboo and wood classification for small-scale users.

2. Methods

Problem Definition

The bending test machine was developed to provide a cost-effective, user-friendly solution for small-scale material testing. Conventional testing equipment is often expensive and inaccessible; thus, the design emphasizes affordability, compactness, and ease of use without sacrificing measurement accuracy. The specifications include a maximum load of 20 kN, automatic flexural rigidity computation, material grading capability, and portability for field applications.

Table 1. Specifications of the Machine

Primary	Secondary	Tertiary Can talk	
Apply a load of up to 20 kN	Portable (the machine can be disassembled and assembled easily)		
Auto calculate flexural rigidity, can automate classify product grading, and display the result	Light	Auto Zero setting	
Easy to set up	Compact (Have every feature inside the machine)	Water resistance	
Can give data load vs displacement	Costs (under 10 million)	Toolbox holder	

Design and Benchmarking

Three conceptual models were developed in SOLIDWORKS, focusing on loading mechanisms, sensor integration, and structural rigidity. Design 1 featured an open frame, Design 2 employed a compact vertical configuration, and Design 3 combined modularity with digital interface integration. A Pugh matrix was applied to benchmark the alternatives against criteria such as manufacturability, stability, and cost. Design 3 achieved the highest weighted score and was selected for prototype fabrication.

Manufacturing

The prototype utilized a hybrid structure of wood and 3D-printed polylactic acid (PLA) to balance strength, precision, and affordability. Structural elements were made from wood, while clamps, actuator mounts, and sensor holders were fabricated using Fused Deposition Modelling (FDM). All components were modelled and assembled in SOLIDWORKS, converted to STL format, and printed under optimized parameters.

Mechanical Properties and Pass n NG grading system

For a 3-point bending test, the equation for the deflection at the point of maximum bending moment, which occurs at the midpoint of the tested specimen, is given by:

$$\delta_{max}(k) = \frac{P(k) \cdot [L]^3}{48 \cdot EI} \tag{1}$$

The mechanical properties that are quantified are the flexural rigidity; therefore, this equation becomes:

$$EI = \left[\frac{1}{48}\right] \left[\frac{P(k)}{\delta_{max}(k)}\right] [L]^3 \tag{2}$$

As shown in the equation, the flexural rigidity of the material specimen is computed by determining the slope of the linear fit model of the scattered data measurement. To obtain the best linear fit model, the method used is computing the model by SVD (Singular Value Decomposition), where in this case, the matrix of scattered load data was decomposed into a unique matrix that consists of,

$$P = U\Sigma V^* \tag{3}$$

Where U and V are unitary matrices, is the diagonal real, non-negative, and *denotes the complex conjugate transpose.

The computation of the mechanical properties is conducted through MATLAB, as the data from Arduino is directly logged to the software. Besides computation, the machine has a main specification of a material grading system that can provide the user with the characteristics of the material defined. It is the grade of the specimen material, with the system as given in the conditioning.

$$PASS\ n\ NG \begin{cases} grade\ [I], & \left\{EI_{std(low)-I} < EI < EI_{std(high)-I}\right\} \\ grade\ [II], & \left\{EI_{std(low)-II} < EI < EI_{std(high)-II}\right\} \\ grade\ [III], & \left\{EI_{std(low)-III} < EI < EI_{std(high)-III}\right\} \\ grade\ [IV], & \left\{EI_{std(low)-IV} < EI < EI_{std(high)-IV}\right\} \end{cases}$$
 (4)

The number of flexural rigidity standards in each grade is defined by the standard given by the user; therefore, if the obtained flexural rigidity of the bamboo specimen is below the lowest standard, it is an indicator that the tested material specimen is not fulfilling the required mechanical properties of the user application.

Stress and Fatigue Analysis

Stress and fatigue analyses were performed on critical components – including the actuator, top base, roller, and connector – to assess load-bearing capability and service life. Finite Element Analysis (FEA) validated analytical results, identifying high-stress regions and potential fatigue failure points. The analyses ensured that each component maintained adequate safety factors under both static and cyclic loading.

Electrical System

The control system integrated an Arduino Mega 2560 with a VL53L0X laser sensor for displacement and a load cell with an amplifier for force measurement. An OLED display provided real-time feedback, while an L298N motor driver controlled the electric linear actuator. A 12 V power supply supported actuator operation, with USB data transfer enabling MATLAB-based computation and visualization.

Prototype Testing

The prototype testing was conducted using two different specimens, namely a plastic ruler and a PVC pipe, to evaluate the system's performance under varying material conditions. During the test, each specimen was subjected to a controlled deflection process while data acquisition was managed through a custom MATLAB script. The code was executed to collect displacement and force data in real time. Following data collection, the results were processed to perform a linear regression analysis using Singular Value Decomposition (SVD), ensuring a robust estimation of the relationship between force and displacement. The regression output was then utilized within MATLAB to compute the flexural rigidity (EI) of each specimen, serving as a key parameter for assessing bending resistance. This approach allowed for a comprehensive evaluation of the prototype's capability in determining material stiffness characteristics.

3. Result and Discussion Synthesis

Three conceptual designs of the bending test machine are developed, focusing on loading mechanisms, sensor integration, and structural stability. As shown in Figure 1, these designs ensure accuracy, durability, and ease of use for effective material testing.

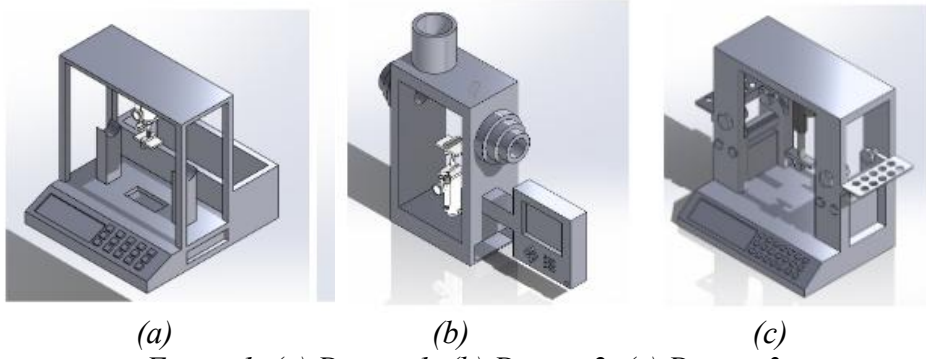


Figure 1. (a) Design 1. (b) Design 2. (c) Design 3

Design 1 (Figure 1a) features a relatively open-frame design with a horizontal testing platform and a central vertical actuator. The layout allows easy sample placement and visibility during testing, which is beneficial for educational and experimental purposes. The sensor integration appears compact and is likely positioned around the actuator, enabling accurate force and displacement measurements. Additionally, this model includes a user interface module at the front, possibly for data input and control, promoting ease of use. However, the open structure may limit protection against external vibrations or dust ingress, which could slightly affect long-term durability in harsh environments.

Design 2 (Figure 1b) adopts a more compact and enclosed vertical configuration. This model emphasizes rigidity and a smaller footprint, which may enhance its portability and precision. The load application mechanism is mounted vertically, and the presence of a control box suggests separation of electronics for safety and thermal management. The rigid frame likely improves stability under higher loads, making this design suitable for more demanding or repeated testing scenarios. However, the compact nature may restrict the size of test specimens and accessibility for adjustments during tests.

Design 3 (Figure 1c) represents a more refined and integrated design, combining the open accessibility of Design 1 with the robustness of Design 2. It includes a central loading mechanism, flanked by symmetrical support columns and a testing bed that appears adjustable. The keyboard and sensor panel suggest real-time monitoring and user interaction, possibly through digital feedback or live plotting. This model also shows modular side panels, which could facilitate component upgrades or maintenance. Design 3 balances user-friendliness, modularity, and performance, making it a strong candidate for both academic and industrial applications.

Benchmarking

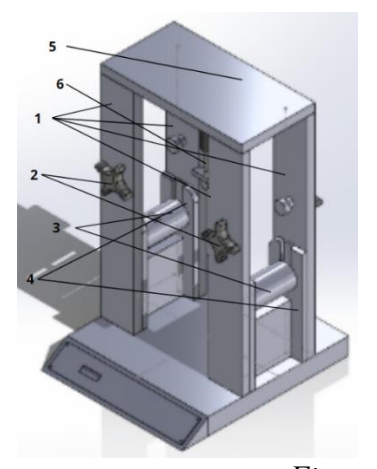
A Pugh Matrix (Table 2) is used to compare the three design models, evaluating their performance based on key criteria. Design 3 is selected as the optimal choice due to its portability, lightweight structure, and compact design, making it the most practical and efficient option for small-scale applications.

Table 2. Pugh Matrix Table Benchmarking all the Models

Primary Specification	Weight	Design 1 (Threshold)	Design 2	Design 3
Apply a load of up to 20 kN	15	0	0	0

Auto calculate flexural rigidity, can automate classify product grading, and display the result	15	0	0	0
Easy to set up	15	0	1	0
Can give data load vs displacement	15	0	0	0
Secondary Specification	Weight	Design 1 (Threshold)	Design 2	Design 3
Portable	7.5	0	-1	-1
Light	7.5	0	-1	1
Compact	7.5	0	-1	1
Costs (under 10 million Rupiah)	7.5	0	0	-1
Tertiary Specification	Weight	Design 1 (Threshold)	Design 2	Design 3
Can talk	2.5	0	0	0
Auto calibration	2.5	0	0	0
Water resistance	2.5	0	0	0
Toolbox holder	2.5	0	0	0
Total Point		0	-2	2
Total Weight		0	-7.5	15

After conducting a benchmarking analysis of three different design alternatives, Design 3 was selected as the most suitable option based on its overall performance, feasibility, and alignment with the project requirements. Several modifications were subsequently implemented to enhance its functionality and compactness, as illustrated can be seen in Figure 4. Following a discussion with the academic advisor, it was determined that the inclusion of a toolbox holder was unnecessary for the intended application, leading to its removal from the design. Additionally, to improve space efficiency and portability, the overall width of the structure was reduced without compromising structural integrity or operational effectiveness. These refinements contributed to a more streamlined and practical final design, while still fulfilling the original objectives of the project.



- 1. Outer Column
- 2. Clamp Hand
- 3. Roller
- 4. Inner Column
- 5. Top Base
- 6. Actuator

Figure 2. Modified Design 3

The components labelled 1 to 6 in Figure 2 represent the main structural and functional parts of the testing assembly. These components are assembled to provide stability, support, and functionality for the testing process, ensuring accurate load application and secure specimen placement throughout the experiment.

Stress analysis

Electric Linear Actuator [27]

The machine is designed to apply a maximum axial load of 20 kN. Consequently, the free-body diagram (FBD) of the actuator, which serves as the primary load-applying mechanism, illustrates that it experiences compression due to the reaction force generated by the applied load, as shown in Figure 3. This reaction force directly affects the actuator's structural integrity and performance, necessitating careful consideration in material selection and system design to ensure reliability and efficiency.



Figure 3. Electric linear actuator FBD

The stress analysis of the linear actuator is calculated due to a 20 kN compressive load. Using the formula of an axial stress with a circular cross section, the stress is found to be 63.66 MPa. The value represents internal forces per unit area that the actuator experiences under the applied load. The safety factor is calculated by comparing the material yield strength (Aluminium 6061 T6) to the applied stress, resulting in a safety factor of 3.78 [28]. This indicates that the actuator can endure nearly four times the current load before reaching its yield point, confirming a safe and reliable design. To validate the analytical result, a finite element analysis (FEA) was conducted, as depicted in Figure 4, allowing for a comparison between the calculated axial stress and the simulated stress distribution under identical loading conditions.

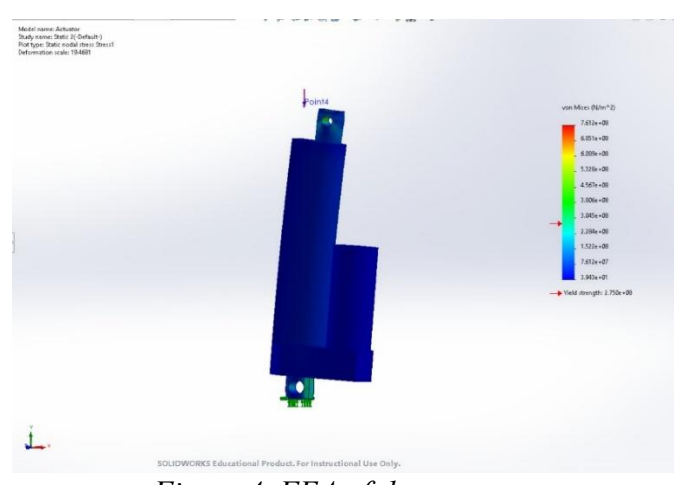


Figure 4. FEA of the actuator

The finite element analysis (FEA) results indicate that the maximum von Mises stress experienced by the actuator reaches approximately 304.5 MPa (3.045 × 10⁸ N/m²). This value exceeds the yield strength of Aluminium 6061-T6, which is 275 MPa, suggesting the potential for plastic deformation under the applied loading condition. As a result, the calculated safety factor from the FEA is less than 1. It implies that the current configuration of the actuator may not sustain the specified load without structural failure. In comparison, the analytical calculation based on the axial stress formula for a circular cross-section subjected to a 20 kN compressive load produced a significantly lower stress value of 22.04 MPa. This corresponds to a safety factor of 10.93, indicating that the actuator could theoretically withstand more than ten times the applied load before reaching the material's yield point. The analytical result suggests a highly conservative and safe design under idealized assumptions.

The notable discrepancy between the analytical and FEA results can be attributed to several key factors. The analytical method assumes idealized conditions, including uniform axial loading and a simplified geometry, while neglecting stress concentrations and detailed boundary conditions. In contrast, the FEA incorporates the actual geometry of the actuator, including fillets, mounting points, and other features that can result in localized stress amplification. Moreover, the analytical approach considers only uniaxial stress. At the same time, the FEA evaluates von Mises stress, which reflects a more comprehensive representation of the stress state by incorporating the combined effects of multi-axial loading.

Top Base

The free body diagram (FBD) of the top base is a simply supported beam subjected to a central downward force, P, representing the load applied by the actuator. The beam is supported at points A and B with corresponding reaction forces RyA and RyB, and bending moments MA and MB, respectively. The distance between the supports is divided equally, with each half-length denoted as L2, indicating a symmetric loading condition. This configuration helps simplify the analysis of internal stresses and reactions due to the applied central load.

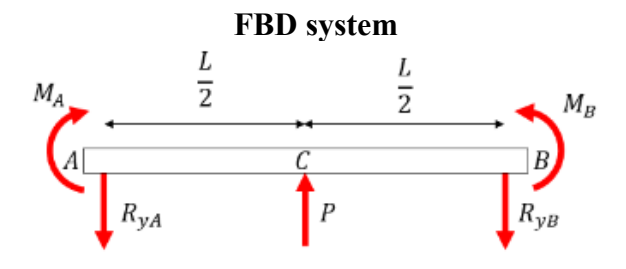


Figure 5. Top Base FBD

Two loading conditions are considered: a 20 kN load applied on a beam of 0.3 m length and 0.02 m width, and a 10 kN load on a beam of 0.6 m length and 0.03 m width. For both cases, the resulting maximum bending stress is calculated to be 125 MPa. This stress value is then compared to the yield strength of the material, which is 215 MPa for stainless steel. From this, a safety factor of 1.72 is determined, indicating that the top base structure can safely withstand the applied load with a reasonable margin before yielding occurs. This analytical result is further validated through finite element analysis (FEA) of

the top base, as shown in Figure 9, which provides a more detailed visualization of the stress distribution under the same loading conditions.

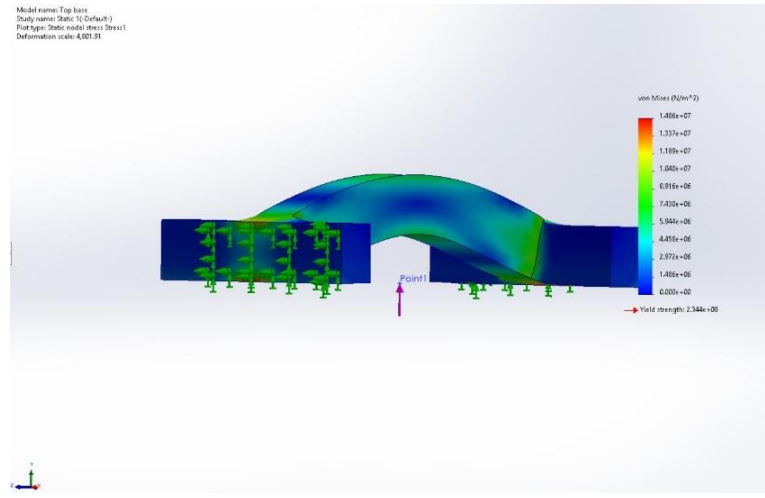


Figure 6. FEA of the top base

The analytical calculation for the top base yields a maximum stress of 125 MPa with a safety factor of 1.72, indicating that the component can safely withstand the applied load. In comparison, the finite element analysis (FEA) shown in Figure 6 reveals a significantly lower maximum von Mises stress of approximately 14.86 MPa, which is far below the yield strength of 234.4 MPa, suggesting a very safe and structurally sound design [28].

Several factors contribute to this notable difference between the analytical and FEA results. First, the analytical method is based on simplified beam theory, which assumes a uniform cross-section and ideal loading and support conditions. It does not account for localized effects such as fillets, cutouts, or mounting features that can redistribute stresses in the actual structure. Second, the analytical model typically considers only a single loading plane and neglects three-dimensional effects, whereas FEA includes all degrees of freedom and can simulate complex boundary conditions and constraints.

Additionally, the analytical calculation often assumes a worst-case scenario to ensure safety, which can lead to conservative results. In contrast, the FEA incorporates detailed material behavior, mesh refinement, and real geometry that allow for a more precise and localized evaluation of stress concentrations. The difference may also be influenced by the actual load path and stiffness distribution in the 3D model, which are not captured in simplified hand calculations. These factors collectively explain why FEA results appear less severe than those predicted analytically, while still confirming the robustness of the design.

Roller

The roller support, as shown in Figure 7, serves a crucial function in distributing the applied load and maintaining structural equilibrium. To determine the reaction force (F), the equilibrium equation for vertical forces is applied. Given that the system is symmetric and subjected to a 10 kN downward force at the center, the reaction forces at both roller supports are equal. By summing the vertical forces, it is found that F = 5 kN at each support.

With the reaction forces determined, the shear force diagram (SFD) and bending moment diagram (BMD) are constructed. The shear force remains constant at 5 kN from the left roller until reaching the 10 kN downward force at the center, causing an abrupt drop to -5 kN. The shear force then remains at -5 kN until it reaches the right roller support, where the 5 kN reaction force restores equilibrium. In terms of bending moments, the maximum bending moment occurs at the center, where the applied force is located. Using the bending moment equation, the peak bending moment is calculated as 285 Nm, which decreases to zero at the supports, forming a triangular distribution.

The stress analysis of the roller part shows that it experiences a bending stress of 13.4 MPa, which increases to a maximum of 18.626 MPa due to a stress concentration at the shoulder fillet. This concentration is characterized by a stress concentration factor of 1.39, which is obtained from the diameter ratio and the fillet radius ratio from the stress concentration graph. Comparing the maximum stress to the yield strength of stainless steel (215 MPa) results in a high safety factor of 11.54, indicating that the roller operates well within safe limits [28]. This high margin suggests the component is structurally robust, withstanding significantly more stress than it currently experiences, which is beneficial for durability and resistance to fatigue. However, it also presents an opportunity for design optimization, such as reducing material usage or weight, depending on the specific performance and cost requirements of the application. The stress analysis of the roller is further validated by the FEA results, as depicted in Figure 10. It confirms the presence of localized stress at the shoulder fillet and supports the high safety factor of 11.54.

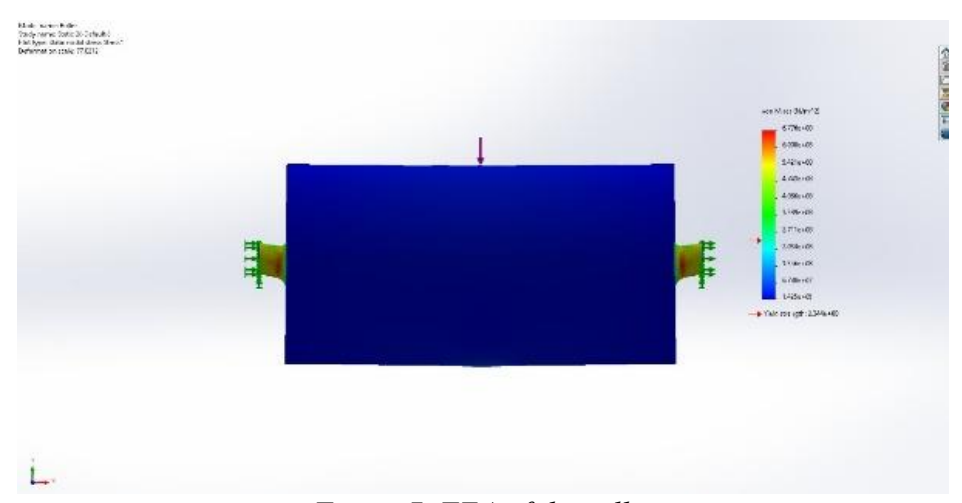


Figure 7. FEA of the roller

The analytical stress analysis of the roller part, which accounts for stress concentration at the shoulder fillet using a factor of 1.39, yields a maximum bending stress of 18.626 MPa and a safety factor of 11.54 against the yield strength of stainless steel (215 MPa), indicating a highly conservative and safe design. However, the finite element analysis (FEA) results shown in Figure 6 demonstrate a significantly higher maximum von Mises stress of approximately 677.6 MPa, far exceeding the material's yield strength of 234.4 MPa.

Connector Actuator to Load Cell

The free body diagram (FBD) of a part of the connector, which is subjected to axial loading, where a tensile force of 10 kN is applied vertically upward at the top hole and an equal force of 10 kN is applied downward at the bottom surface. These opposing forces place the component in a state of static equilibrium, resulting in zero net external force and no acceleration. The applied loads induce internal forces within the material, which resist the external loading and are distributed throughout the component's cross-section. To ensure structural reliability and identify potential failure regions, it is necessary to perform a stress analysis based on this loading condition by assuming it is a plate.

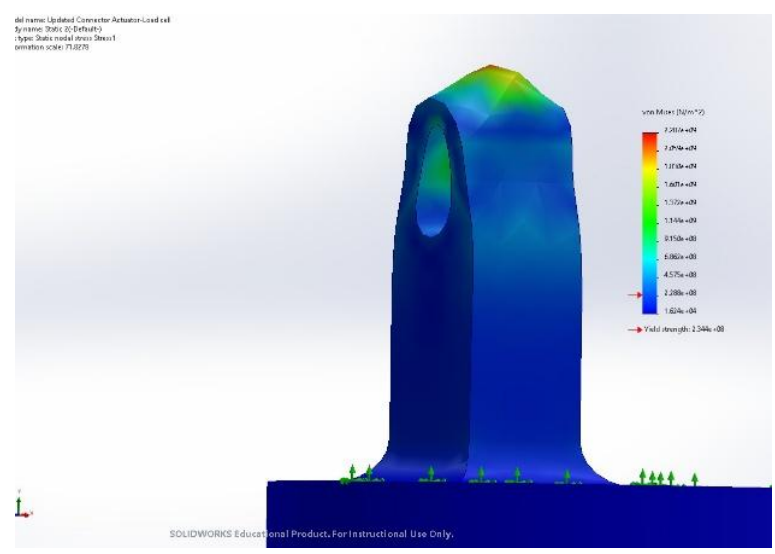


Figure 8. FEA of Connector Actuator to Load Cell

The FEA results shown in the figure reveal that the maximum von Mises stress reaches approximately 2.287×10^8 N/m² (228.7 MPa), which is slightly higher than the analytical stress calculation of 210 MPa. This discrepancy is expected due to the more detailed geometry and boundary condition modelling in FEA, which accounts for stress concentrations—particularly near the hole where the load is applied. The material's yield strength is 234.4 MPa. The safety factor is approximately 1.025 with a maximum FEA stress of 228.7 MPa. It almost aligns with the analytical safety factor of 1.02. While both approaches indicate the design is just below yielding, the minimal safety margin suggests that any variation in material properties, load spikes, or imperfections may lead to component failure [28]. Thus, both the FEA and analytical results highlight the need for either material selection with higher yield strength or geometric optimization to improve the safety factor.

Fatigue Analysis

Analysis was conducted on 4 components of the machine to observe the fatigue strength. Each of these components is calculated for its endurance strength and fatigue safety factor, and if its safety factor is below 1, then its life cycle is calculated.

Roller

The roller, made from stainless steel with an ultimate tensile strength (Sut) of 505 MPa, is expected to have an endurance limit (Se) of 252.5 MPa. Considering it has a

machined surface finish, a correction factor is applied, along with adjustments for size, loading type, temperature, and reliability. The roller experiences bending loads at room temperature and is assumed to have 95% reliability, with a stress concentration factor considered due to its geometry. Taking all these factors into account, the corrected endurance strength (Se') is calculated to be approximately 189.9 MPa. With a resulting fatigue safety factor of 10.19, the roller is expected to have an infinite life under the given loading conditions.

Top Base

The top base, constructed from machined stainless steel, shares the same ultimate tensile strength and surface finish factor as the rollers. Given its non-rotating rectangular geometry, a different size factor is applied based on its dimensions. The component operates under bending loads in a room temperature environment, and a conservative reliability factor of 95% is used. As the top base has no fillets or notches, the stress concentration factor is considered to be 1. Taking all these factors into account, the corrected endurance strength is calculated to be approximately 142.92 MPa. With a resulting fatigue safety factor of 1.14, the top base is expected to achieve an infinite life under the given operating conditions.

Connector

The connector, made from stainless steel, shares the same surface finishing factor as the roller and top base. Treated as a rectangular plate, its size factor is determined accordingly. Subjected to axial loading from the actuator, the connector has a reduced loading factor, while the temperature and reliability factors remain standard, assuming room temperature operation and 95% reliability. A stress concentration exists due to a circular hole, which increases the effective fatigue load through a notch sensitivity factor. After applying all Marin factors, the corrected endurance strength of the connector is found to be 148.42 MPa, resulting in a fatigue safety factor of 0.7. This indicates that the connector is not expected to have an infinite life, and it can fail due to fatigue after approximately 118,256 cycles.

For the linear actuator, which is made of Aluminum 6061 with a machined finish, the component is modelled as a non-rotating cylindrical specimen under axial load. With no notch sensitivity and standard room temperature and reliability conditions, the corrected endurance strength is calculated as 90.2 MPa, resulting in a fatigue safety factor of 4.09. This confirms that the linear actuator is expected to have an infinite life. Among the four analysed components, the connector is identified as the most critical in terms of fatigue performance, being the only part with a finite fatigue life.

Manufacturing Results

The manufacturing results reflect several design refinements made based on the prior stress analysis. Initially, the top base was designed as a flat plate. However, due to the high stress concentration observed during simulation, the design was revised using an overdetermined support concept, resulting in an "I" shape profile that significantly improved structural integrity while minimizing deflection. Additionally, the actuator dimensions were updated to a larger model to meet the required loading capacity. Consequently, the height of the outer columns had to be adjusted from the original 40 cm to 63 cm to accommodate this change. The outcome of the manufacturing process, incorporating these improvements, can be seen in Figure 14.

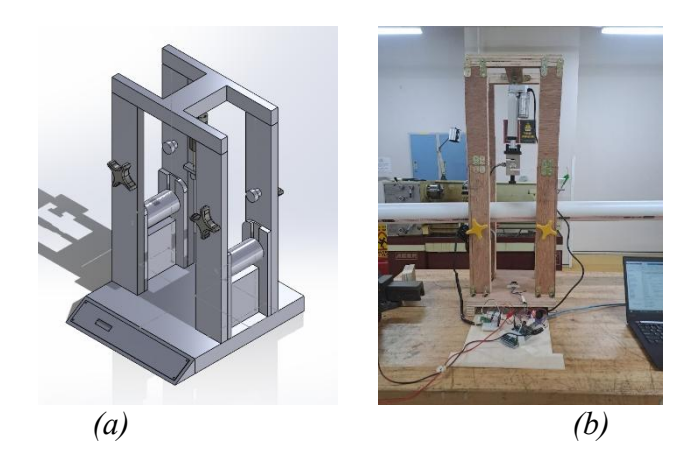


Figure 9. (a) Redesign of Design 3 (b) Prototype of the bending test machine

Electrical Components

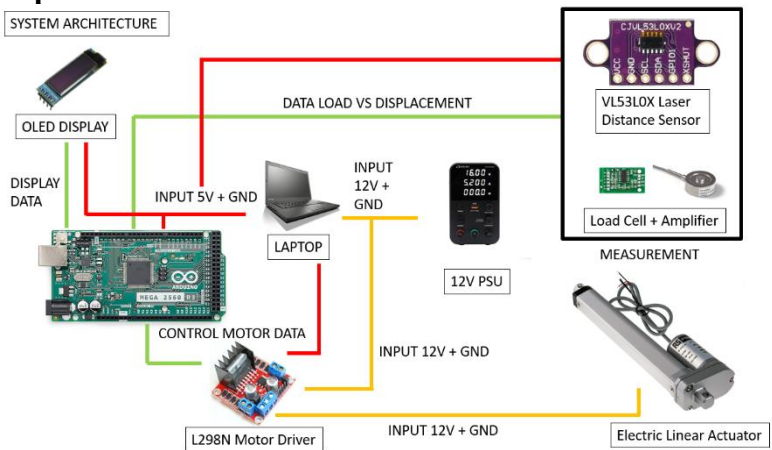


Figure 10. Electrical Hardware

Figure 10 illustrates a system architecture for measuring mechanical properties using an Arduino Mega 2560 as the central controller. The system collects load and displacement data through a VL53L0X laser distance sensor and a load cell with an amplifier, with the results displayed on an OLED screen. Power is supplied via a 12V power supply unit (PSU) for the actuator and motor driver, while the Arduino and other low-power components receive power through a USB connection from a laptop. An L298N motor driver controls the electric linear actuator, which applies a bending force to the test specimen. The Arduino processes the sensor data, controls the actuator, and updates the OLED display, enabling automated testing for evaluating material stiffness or modulus.

Testing Results

Testing elastic specimen (high deflection)

The specimen used for this testing is a ruler, which has a higher deflection number. The deflection is high, so the VL53L0X sensor can detect higher deflection data. The purpose is to find the ideal data result of this machine, lower load for the actuator, and specimen length ratio to simulate the bending condition.

The test results from the bending test machine are a series of data consisting of load variables obtained from load cell measurements and displacement variables obtained from laser sensor VL53L0X measurements. Measurements of both variables are carried out simultaneously with a zeroing system or a system where, in the initial condition, both sensors are recorded as zero values. Therefore, when both sensors detect changes in the specimen, the changes are recorded from the reference point that has been defined.

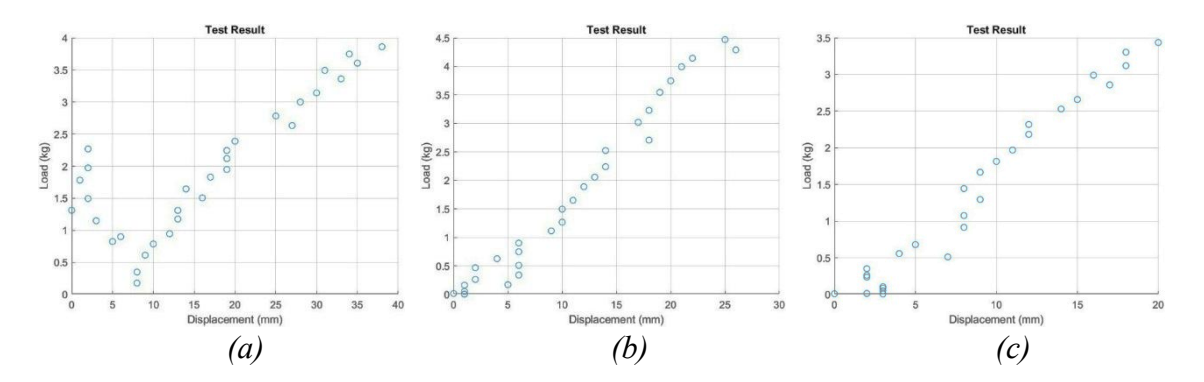


Figure 11. Testing result data. (a) First testing without zeroing, (b) Second testing, (c) Third testing.

In the first test, Figure 11a, the zeroing system was not used; therefore, the first few indexes in the data display noise at high points in each parameter. In the next two tests, Figure 11b and 11c, the zeroing system is used so that the initial index of the measurement data starts from zero.

Testing stiffer specimen (low deflection)

The next tested specimen is a PVC pipe, which has similar geometrical properties to bamboo. But due to the prototyping, the testing is not ideal for this specimen.

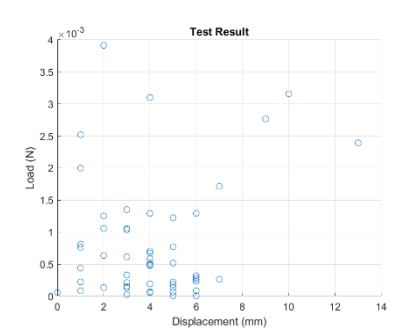


Figure 12. Raw data

As shown in Figure 12, the data has a lot of noise that overlaps with the linearity data. It occurs due to the sensor distance reading the fluctuation in the unchanged distance of the deflection, which can distort the data result.

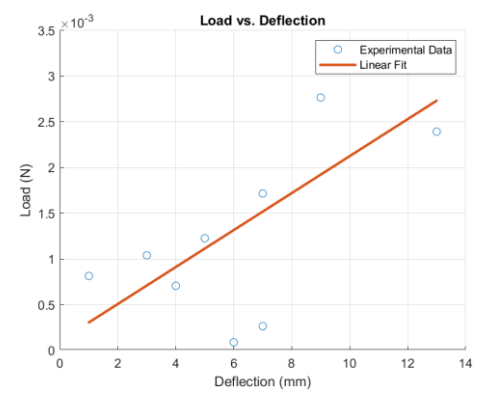


Figure 13. Pre-processed data and Mechanical properties computation

To overcome this, data preprocessing is necessary to eliminate the noise from the linear data to increase the linear fit model accuracy, as shown in Figure 13. The result is

- a. Slope(P/d): 0.000202 N/m
- b. Computed Flexural Rigidity (EI): 51.268798 Pam4
- c. Grade: II

4. Conclusion

This research presented the design, analysis, and fabrication of a portable, low-cost bending test machine intended for characterizing the mechanical properties of wood and bamboo. Three conceptual configurations were developed and evaluated through a Pugh matrix, with Design 3 identified as the optimal model due to its superior balance of structural rigidity, compactness, and operational simplicity. Detailed analytical and finite element analyses were conducted on critical components (the actuator, top base, roller, and connector) to assess static strength and fatigue performance. Results indicated that most components satisfied structural safety criteria, while the connector exhibited limited fatigue life, suggesting the need for material or geometric optimization. The final prototype, integrating an Arduino-based control system with laser and load sensors, demonstrated reliable performance in measuring load-deflection responses and calculating flexural rigidity after data reprocessing. The findings confirm that the proposed system provides a technically viable, accurate, and scalable platform for small-scale mechanical testing and material classification, supporting broader applications in sustainable construction and material research.

References

- [1] S. Abramowitch and D. Easley, "Introduction to classical mechanics," in *Elsevier eBooks*, 2016, pp. 89–107. doi: https://doi.org/10.1016/B978-0-12-803228-2.00004-0.
- [2] H. Farhat, "Materials and coating technologies," in *Elsevier eBooks*, 2021, pp. 63–87. doi: https://doi.org/10.1016/B978-0-12-821834-1.00007-1.
- [3] X. Zeng, S. Wen, M. Li, and G. Xie, "Estimating Young's modulus of materials by a new Three-Point bending method," *Advances in Materials Science and Engineering*, vol. 2014, pp. 1–9, Jan. 2014, doi: https://doi.org/10.1155/2014/189423.
- [4] N. Martin-Nelson, B. Sutherland, M. Yancey, C. S. Liao, C. J. Stubbs, and D. D. Cook, "Axial variation in flexural stiffness of plant stem segments: measurement

- methods and the influence of measurement uncertainty," *Plant Methods*, vol. 17, no. 1, Oct. 2021, doi: https://doi.org/10.1186/s13007-021-00793-8.
- [5] S. K. Mukarramah, A. G. Abdullah, and S. Sumarto, "Low-cost bending test laboratory kit," *IOP Conference Series Materials Science and Engineering*, vol. 830, no. 4, p. 042087, Apr. 2020, doi: https://doi.org/10.1088/1757-899x/830/4/042087.
- [6] M. Misganew and N. Peddinti, "Testing the bending strength of solid bamboo and hollow bamboo particleboard," in *Springer eBooks*, 2019, pp. 550–561. doi: https://doi.org/10.1007/978-3-030-15357-1 44.
- [7] P. Liu, Q. Zhou, F. Fu, and W. Li, "Bending Strength Design Method of Phyllostachys edulis Bamboo Based on Classification," *Polymers*, vol. 14, no. 7, p. 1418, Mar. 2022, doi: https://doi.org/10.3390/polym14071418.
- [8] P. Xie, W. Liu, Y. Hu, X. Meng, and J. Huang, "Size effect research of tensile strength of bamboo scrimber based on boundary effect model," *Engineering Fracture Mechanics*, vol. 239, p. 107319, Sep. 2020, doi: https://doi.org/10.1016/j.engfracmech.2020.107319.
- [9] Y. Deng and C. Peng, "Experimental study on bending mechanical properties of moso bamboo," *E3S Web of Conferences*, vol. 293, p. 03010, Jan. 2021, doi: https://doi.org/10.1051/e3sconf/202129303010.
- [10] L. Tian, J. Wei, J. Hao, and Q. Wang, "Characterization of the flexural behavior of bamboo beams," *JOURNAL OF RENEWABLE MATERIALS*, vol. 9, no. 9, pp. 1571–1597, Jan. 2021, doi: https://doi.org/10.32604/jrm.2021.015166.
- [11] D. Trujillo, S. Jangra, and J. M. Gibson, "Flexural properties as a basis for bamboo strength grading," *Proceedings of the Institution of Civil Engineers Structures and Buildings*, vol. 170, no. 4, pp. 284–294, Dec. 2016, doi: https://doi.org/10.1680/jstbu.16.00084.
- [12] M. G. Rifqi, M. S. Amin, and R. R. Bachtiar, "Mechanical properties of Culm Bamboo Endemic Banyuwangi based on tensile strength test," *Proceedings of the International Seminar of Science and Applied Technology (ISSAT 2020)*, Jan. 2020, doi: https://doi.org/10.2991/aer.k.201221.066.
- [13] S. Kaminski, A. Lawrence, and D. Trujillo, "Structural use of bamboo. Part 1: Introduction to bamboo," *The Structural Engineer*, vol. 94, no. 8, pp. 40–43, Aug. 2016, doi: https://doi.org/10.56330/PNSC8891.
- [14] D. Yang *et al.*, "Length effect on bending properties and evaluation of shear modulus of parallel bamboo strand lumber," *European Journal of Wood and Wood Products*, vol. 79, no. 6, pp. 1507–1517, Jun. 2021, doi: https://doi.org/10.1007/s00107-021-01714-1.
- [15] T. Mouka, E. G. Dimitrakopoulos, and R. Lorenzo, "Effect of a longitudinal crack on the flexural performance of bamboo culms," *Acta Mechanica*, vol. 233, no. 9, pp. 3777–3793, Aug. 2022, doi: https://doi.org/10.1007/s00707-022-03314-3.
- [16] Kumar, A., Behura, A.K., Rajak, D.K., Behera, A., Kumar, P., Kumar, R., "Fundamental concepts of bamboo: Classifications, properties and applications", pp. 39-62, 2020, doi: https://doi.org/10.1007/978-981-15-8489-3 3.
- [17] S. Greco, M. Maraldi, and L. Molari, "Grading bamboo through four-point bending tests. A report on six species of Italian bamboo," *Construction and Building Materials*, vol. 404, p. 133168, Sep. 2023, doi: https://doi.org/10.1016/j.conbuildmat.2023.133168.

- [18] Y. Goyal, "Comparative study of Microcontoller: ARDUINO UNO, RASPBERRY PI 4, ESP 32," *International Journal for Research in Applied Science and Engineering Technology*, vol. 12, no. 7, pp. 588–592, Jul. 2024, doi: https://doi.org/10.22214/ijraset.2024.63598.
- [19] J. Pustavrh, M. Hočevar, P. Podržaj, A. Trajkovski, and F. Majdič, "Comparative study of a hydraulic, pneumatic and electric linear actuator system," *Research Square (Research Square)*, Jul. 2023, doi: https://doi.org/10.21203/rs.3.rs-3184855/v1.
- [20] V. Nasir, S. Ayanleye, S. Kazemirad, F. Sassani, and S. Adamopoulos, "Acoustic emission monitoring of wood materials and timber structures: A critical review," *Construction and Building Materials*, vol. 350, p. 128877, Aug. 2022, doi: https://doi.org/10.1016/j.conbuildmat.2022.128877.
- [21] A. Fernández, F. J. Rescalvo, A. Cruz, C. Abarkane, and J. M. Santiago, "Acoustic emission analysis of raw bamboo subjected to tensile tests," *Mechanics of Advanced Materials and Structures*, vol. 28, no. 13, pp. 1389–1397, Oct. 2019, doi: https://doi.org/10.1080/15376494.2019.1675105.
- [22] J. Stiefvater *et al.*, "Dual-Use strain sensors for acoustic emission and Quasi-Static bending measurements," *Sensors*, vol. 24, no. 5, p. 1637, Mar. 2024, doi: https://doi.org/10.3390/s24051637.
- [23] N. Y. Tombal and T. V. Mumcu, "A Comparison of Ultrasonic and Laser Sensor-Based SLAM Algorithms Applied to Carlike Vehicles," *Electrica*, vol. 24, no. 1, pp. 228–237, Jan. 2024, doi: https://doi.org/10.5152/electrica.2024.23075.
- [24] S. Han *et al.*, "Numerical simulation of angled surface crack detection based on laser ultrasound," *Frontiers in Physics*, vol. 10, Aug. 2022, doi: https://doi.org/10.3389/fphy.2022.982232.
- [25] S. Okubo, N. Parikesit, K. Harashina, D. Muhamad, O. S. Abdoellah, and K. Takeuchi, "Traditional perennial crop-based agroforestry in West Java: the tradeoff between on-farm biodiversity and income," *Agroforestry Systems*, vol. 80, no. 1, pp. 17–31, Jul. 2010, doi: https://doi.org/10.1007/s10457-010-9341-8.
- [26] G. A. Erfani, Z. Abidin, and V. Violet, "PRODUKTIVITAS, RENDEMEN DAN KONTRIBUSI KERAJINAN BAMBU (Bambusa sp) TERHADAP PENDAPATAN DI DESA TAMBAK BARU KECAMATAN MARTAPURA TIMUR KABUPATEN BANJAR," *Jurnal Sylva Scienteae*, vol. 3, no. 3, p. 486, Jul. 2020, doi: https://doi.org/10.20527/jss.v3i3.2182.
- [27] ASM Aerospace Specification Metals Inc., "ASM Material Data Sheet." (accessed May 15, 2025).
- [28] Sunrise, "Yield strength of aluminum alloys," Sunrise Metal Aluminium Die Casting Expert, Apr. 03, 2024. (accessed May 15, 2025).